ISSN 0036-0244, Russian Journal of Physical Chemistry A, 2015, Vol. 89, No. 8, pp. 1429–1433. © Pleiades Publishing, Ltd., 2015.
Original Russian Text © A.E. Galashev, V.A. Polukhin, 2015, published in Zhurnal Fizicheskoi Khimii, 2015, Vol. 89, No. 8, pp. 1282–1286.

PHYSICAL CHEMISTRY
OF NANOCLUSTERS AND NANOMATERIALS

Computer Modeling of the Structure and Properties of Mercury Films on Graphene

A. E. Galashev[a] and V. A. Polukhin[b]

[a] *Institute of High Temperature Electochemistry, Russian Academy of Sciences, Ural Branch, Yekaterinburg, 620137 Russia*
[b] *Institute of Materials Science and Metallurgy, Ural Federal University, Yekaterinburg, 620002 Russia*
e-mail: galashev@ecko.uran.ru

Received October 17, 2014

Abstract—The physical properties of mercury films on partially hydrogenated imperfect graphene are studied by means of molecular dynamics at 300 K. Films prepared on the basis of three various types of the atomic interaction potential for mercury and other constant interaction potentials are considered. It is shown that the one most promising is the Schwerdtfeger potential function, at which mercury atoms do not fall into the divacancies present on graphene and atom packing with the lowest energy are realized in a liquid film and the film gradually folds into a drop. The horizontal and vertical mobilities of mercury atoms, the radial distribution function of Hg film, and the roughness of graphene are calculated.

Keywords: graphene, mercury film, interaction potential, substrate roughness.
DOI: 10.1134/S0036024415080129

INTRODUCTION

Environmental pollution with heavy metals is a global problem [1, 2], due to its detrimental consequences for health [3]. Composite membranes based on graphene for the accumulation of mercury have were proposed in [4]. The structure and physical properties of liquid mercury–graphene interfaces remain unstudied; meanwhile, the prospect of using graphene as a filter demands their study. Liquids with isotropic pair interactions encounter vibrational interface structures at temperatures close to melting point T_m, providing that the T_m/T_c ratio (where T_c is the critical temperature) is low. The melting point of bulk mercury $T_m = 234$ K.

Cold liquid metals such as Hg and Ga have low $T_m/T_c = 0.13$ and 0.15, respectively. Molecular dynamic (MD) modeling reveals their nonmonotonous density profiles near the liquid mercury/vapor interface [5]. On the other hand, the interface range has a non-zero thickness that depends on temperature. Calculating the properties of a Hg liquid–vapor interface with clear allowance for the dependence of the potential of density did not result in satisfactory agreement with the experimental data on ionic and electron density distributions orthogonal to the surface or on the reflection coefficient [6].

Theoretical study of liquids of the Hg type requires knowledge of the effective atomic potential, which allows correct predictions of the liquid/vapor phase diagram in temperature–density coordinates. Out of all the proposed potential functions for mercury, it is difficult to choose one on whose basis the structure of liquid mercury on graphene can be reproduced satisfactorily. The structure of solid metals in contact with graphene (e.g., deposited copper films) has been studied more thoroughly [7].

The aim of this work was to choose an effective pair potential that allows reproduction of the structural, thermodynamic, and kinetic properties of mercury films deposited on graphene in a molecular dynamics model.

COMPUTER MODEL

Our calculations were performed according to conventional molecular dynamics. Three types of empirical potentials were used that describe carbon–carbon (in graphene), mercury–mercury, and mercury–carbon interactions. The Tersoff potential was taken as the basis for our representation of the interactions in graphene [8, 9]:

$$U^{\mathrm{Ter}} = \frac{1}{2}\sum_i \sum_{j\neq i} f_c(r_{ij})\{f_R(r_{ij}) + b_{ij} f_A(r_{ij})\}, \qquad (1)$$

$$f_R(r) = A\exp(-\lambda_1 r),$$

$$f_c(r) = \begin{cases} 1, & r < R, \\ \frac{1}{2} + \frac{1}{2}\cos\frac{\pi(r-R)}{S-R}, & R < r < S, \\ 0, & r > S, \end{cases}$$

$$f_A(r) = -B\exp(-\lambda_2 r),$$

$$b_{ij} = (1+\beta^n\varsigma_{ij}^n), \quad \varsigma_{ij} = \sum_{k\neq i,j} f_c(r_{ik})g(\theta_{ijk}),$$

$$g(\theta) = 1 + \frac{c^2}{d^2} - \frac{c^2}{d^2 + (h-\cos\theta)^2}.$$

Here, indices i, j, and k indicate carbon atoms; r_{ij}, the length of an i–j bond; θ_{ijk}, the angle between the bonds i–j and j–k. The parameters of Eq. (1) were taken from [9], except for the S value.

The transition to modeling two-dimensional systems (e.g., graphene) with covalent bonds requires the modification of this potential [10]. In this model, the maximum inclusion (S) of covalent interaction was increased from 0.21 to 0.23 nm. Beyond covalent interactions, there was very weak attractive Lennard–Jones interaction with the parameters of [10]. In order to avoid rotation of our graphene sheet, braking with force $-dV_{ij}(\Omega_{kijl})/dr_{ij}$ was employed at each atomic junction of graphene; torsional potential $V_{ij}(\Omega_{kijl})$ was determined in [10].

The modeling of mercury adsorption on surface requires exact potentials of Hg–Hg and Hg-substrate interaction. Potentials presented as pair interactions are usually used to describe adsorption. The Lennard–Jones potential (LJ) is the simplest of these. The parameters of this potential were chosen according to the data on the viscosity of gaseous mercury [11].

The Silver–Goldman potential (SG) is adjusted to ab initio data and provides good agreement with experimental data on spectroscopic constants [12]. The SG potential is based on the Hartree–Fock model of dispersion,

$$V_{SG}(r) = \exp(\alpha - \beta r - \gamma r^2) - f_c(r)\left(\sum_{n=3}^{5}\frac{C_{2n}}{r^{2n}}\right), \quad (2)$$

where

$$f_c(r) = \exp\left[-(1.28r_c/r - 1)^2\right], \quad r < 1.28r_c$$
$$= 1.0, \quad r \geq 1.28r_c. \quad (3)$$

The parameters of this potential are given in [12].

The Schwerdtfeger pair potential (Sch) reproduces the main properties of mercury such as the melting point and density of liquid Hg quite well. The Sch potential is based on ab initio calculations and has the form [13]

$$V_{Sch}(r) = U_{Sch}(\lambda r) = \sum_{j=3}^{9} a_2^* r^{-2j}, \quad (4)$$

where U_{Sch} is the original Schwerdtfeger potential for mercury [13] and $\lambda = 1.167$ is used for adjusting to the density of liquid Hg at $T = 300$ K. Parameters a_{2j}^* are given in [13].

Graphene–mercury interaction was represented by the LJ potential with the parameters of [13]. On a graphene sheet containing 406 C atoms, 50 Hg atoms were deposited in a random manner. The resulting system was then set to equilibrium in MD calculations with a period of 200000 time steps ($\Delta t = 0.2$ fs). The numerical solution to the equations of motion was found according to the fourth-order Runge–Kutta method.

Divacancies are one of the most widespread defects in graphene. The presence of such defects remarkably enhances the coupling of graphene with a deposited metal. In present model, nine divacancies were formed nearly uniformly on a 3.4 × 2.8 nm graphene sheet. The hydrogenation of graphene results in slight surface ribbing, which also increases the linkage between metal and graphene. Preliminary partial hydrogenation strengthened the graphene edges and stabilized divacancies. A hydrogen atom was effectively added to each boundary C atom (including those in the vicinities of divacancies). More specifically, an entire CH group was considered in considering interactions, rather than individual H atoms. This group interacted with C atoms [14], other CH groups [15], and Hg atoms [12] through the LJ potential. Fourteen CH groups were arranged along the perimeter of each divacancy. Each CH group was described according to monoatomic scheme in [14]. This general scheme was designed in developing translated force fields used to predict the thermodynamic properties of complex molecules [16].

The self-diffusion coefficient was determined via the mean-square displacement of Hg atoms as

$$D = D_{xy} + D_z = \lim_{t\to\infty}\frac{1}{2\Gamma t}\left\langle[\Delta\mathbf{r}(t)]^2\right\rangle_n, \quad (5)$$

where $\Gamma = 3$ is the dimensionality of space. The symbol $\langle\ldots\rangle$ indicates time averaging and n is the number of time intervals for the determination of $\left\langle[\Delta\mathbf{r}(t)]^2\right\rangle_n$. The time average was determined by averaging five curves, each of which was calculated at an interval of 40 ps (or $200000\Delta t$). The surface roughness (or mean deviation of the profile) was calculated as

$$R_a = \frac{1}{N}\sum_{i=1}^{N}|z_i - \overline{z}|, \quad (6)$$

where N is the number of junctions (atoms) on the graphene surface, z_i is the level of atom i, and $\overline{z}$ is the level of the graphene surface; the z_i and $\overline{z}$ values were determined for the same moment in time.

Energies U_{Hg-Hg} and U_{Hg-C} of a liquid mercury film on graphene for three potentials

Energy	Potentials		
	LJ	Sch	SG
U_{Hg-Hg}, eV	−0.0236	−0.0280	−0.0011
U_{Hg-C}, eV	−0.0154	−0.0121	−0.0148

RESULTS AND DISCUSSION

The full energy of perfect single-sheet graphene obtained at $T = 300$ K was −7.02 eV, in agreement with quantum-mechanical calculations (−6.98 eV) [17]. Energy U_{Hg-Hg} of Hg–Hg interaction in the film, which was set after equilibrating the system with the LJ potential, was one-third that of the bond energy in a Hg_2 dimer, determined with the same potential [12]. The analogous energies U_{Hg-Hg} for two other potentials with energies of mercury–graphene interaction U_{Hg-C} are given in the table. It can be seen the highest absolute values of energy U_{Hg-Hg} were obtained for the Sch potential; the lowest, for the SG potential. On the other hand, the best cohesion between mercury and graphene was provided by the LJ potential; the worst, by the Sch potential.

Using the LJ, Sch, and SG potentials for mercury yielded metal films of various structures on graphene. the LJ potential yields a denser packing of Hg atoms, while the SG potential yields more loose and uniform packing. There is a tendency toward the vaporization of atoms at temperatures as low as 300 K for the SG potential. The configuration of the H–graphene–Hg-film system obtained with the Sch potential is given in Fig. 1 for the moment of 200 ps. At this time, graphene had a slight ribbing that could be detected from the deviation of boundary C atoms from the even row of H atoms built along the initial coordinates of the CH-groups. The Hg film was in this case quite uniform. However, it did not spread over the entire graphene surface; rather, it gathered into an elongated drop that was flattened to graphene. None of the Hg atoms spilled onto the other side of graphene through a divacancy, though several metal atoms did get stuck in defects. The movement of Hg atoms to the other side of the graphene was observed for two other potentials, though these spills were less than 0.08 nm long. The Sch potential was the one that was best from the viewpoint of retaining Hg atoms on graphene.

Due to the thinness of the film, its z-profile of density was determined quite roughly and revealed no oscillations for the three types of potentials. However, the distribution of Hg atoms over the graphene surface was neither homogeneous nor uniform for the considered cases. The greatest tendency toward the formation of dense clusters in a film was characteristic for the system created using the LJ potential for mercury (Fig. 2), where the first three peaks of function $g(r)$ were the highest and well resolved. A tighter and more compact structure was characteristic of the film obtained using the Sch potential: only the first four peaks of function $g(r)$ were clearly resolved. In this case, however, the Hg film was also shown to be very

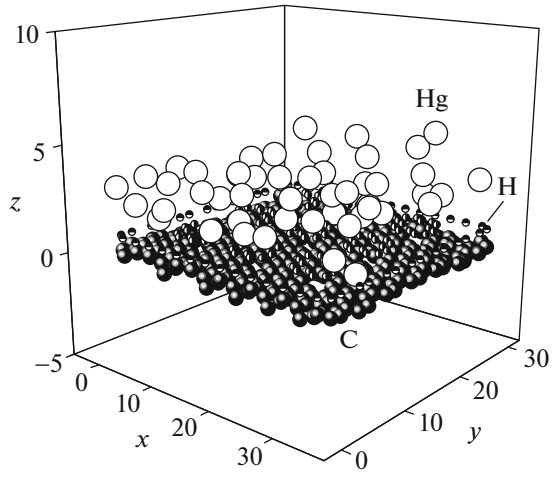

Fig. 1. Configuration of a mercury film on a modified graphene system, obtained at the moment of 200 ps. The positions of H atoms correspond to the coordinates of CH-groups reduced to one point at the initial moment in time.

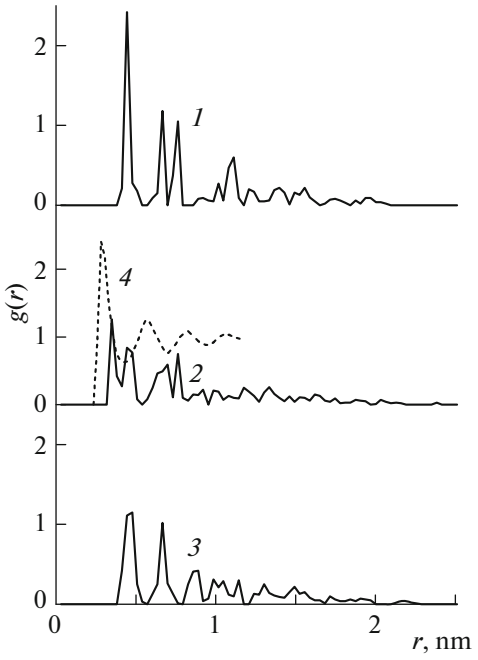

Fig. 2. Radial distribution functions of mercury films on graphene, obtained with the atomic interaction potentials (*1*) LJ, (*2*) Sch, (*3*) SG; (*4*) $g(r)$ of bulk liquid mercury (MD calculations) [5].

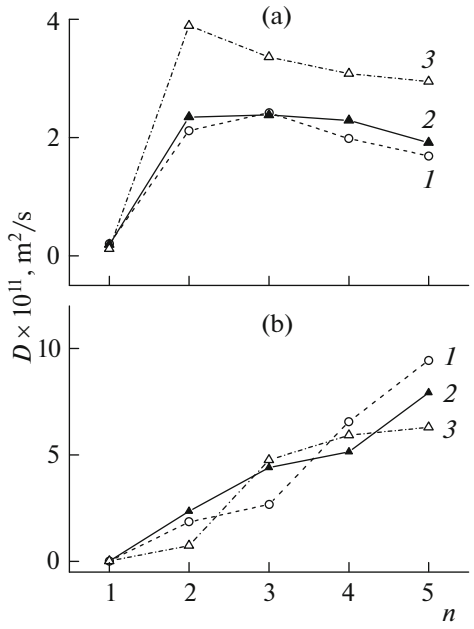

Fig. 3. (a) Horizontal and (b) vertical components of the mobility coefficients of Hg atoms in mercury films on graphene, obtained using the atomic potentials (*1*) LJ, (*2*) Sch, (*3*) SG; n is the number of the interval in which coefficients D_{xy} and D_z were determined.

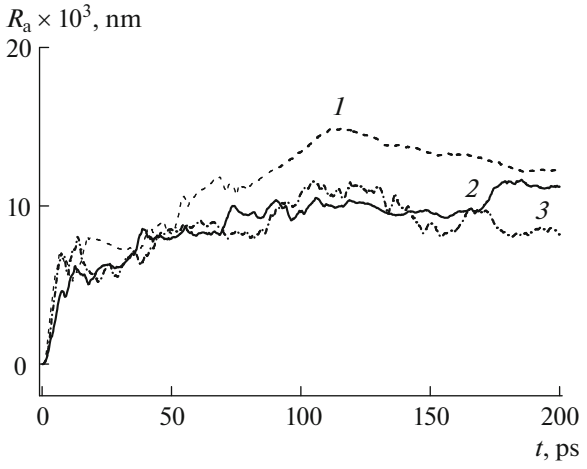

Fig. 4. Evolution of the roughness of graphene coated by mercury films, obtained using the atomic potentials (*1*) LJ, (*2*) Sch, and (*3*) SG.

loose, so the first peak of function $g(r)$ shifted ~0.07 nm away from the position of the corresponding peak of function $g(r)_{\text{liquid}}$ for bulk liquid mercury [5]. The four first peaks of the film were distributed between the positions of the first and third peaks of function $g(r)$ for liquid mercury.

The radial distribution function for the film obtained with the SG potential had the greatest (~0.17 nm, relative to the position of peak of $g(r)_{\text{liquid}}$) shift of the first peak. The emergence of the second peak $g(r)$ of this film only slightly anticipated the position of the third peak of this function for the Hg film formed using the Sch potential.

The specificity of the geometry of system requires individual consideration of horizontal and vertical mobility of Hg atoms. The behavior of the horizontal D_{xy} and vertical D_z components of the self-diffusion coefficient of Hg when calculating at the time intervals n of 40 ps with different atomic interaction potentials for mercury is shown in Fig. 3. Component D_{xy} grows only up to $n = 2$. At subsequent time intervals, D_{xy} usually stabilized or fell inconsiderably. This behavior of D_{xy} was due mainly to the initial sealing of the Hg film and the subsequent retention of its density. The highest values of D_{xy} were obtained using the SG potential, while the lowest values were obtained with the LJ potential. The Sch potential produced most stable values of D_{xy} at $n \geqslant 2$. In addition, these values did not differ appreciably from the D_{xy} value obtained with the LJ potential. The vertical component of the mobility of Hg atoms behaved differently for all considered potentials. In all cases, the D_z value grew nonmonotonously along with n. Finally, the maximum value of D_z was reached with the LJ potential; the minimum value, with the SG potential. In this context, the situation is inverse to the behavior of component D_{xy} at high n. Another feature of dependence $D_z(n)$ was determined by the tendency toward vaporization from the film of Hg atoms with each potential. For all three of our model potentials, self-diffusion coefficients were obtained that were lower than the experimental value of D (15.9×10^{-11} m^2/s at T = 298 K) for liquid mercury [18]. Somewhat better agreement with the calculated values of $D = D_{xy} + D_z$ was achieved when D was determined via nonelastic neutron scattering on liquid mercury (14.3×10^{-11} m^2/s at T = 297 K) [19].

Like hydrogenation, a mercury film that forms on graphene affects its 3D structure (i.e., its roughness R_a). In calculations, the R_a value increases for Hg films that form with all three potentials (Fig. 4). The highest R_a values are characteristic of graphene with a metal film obtained via Lennard–Jones interaction. The Hg films created with the Sch and SG potentials have similar R_a values throughout all calculations. At the final step of calculation, however, the R_a value for the Hg film formed as the result of using the SG potential becomes lower.

The forces of cohesion between mercury and graphene atoms are weak, compared to the ones between mercury atoms. Mercury tends toward its natural boundary angle, wetting is terminated, and mercury gradually consolidates into individual drops. This phenomenon is largely reproduced using the Sch potential. A tendency toward drop formation is also observed for the LJ and SG potentials, but in these cases there are considerably more individual atoms on the graphene surface, and each drop has a less distinct profile. For real mercury, vaporization proceeds at temperatures above 291 K. Cohesion with modified graphene does not allow Hg atoms to detach from the film at distances much greater than atomic at 300 K. However, the tendency toward the vaporization of Hg atoms is still observed in model systems and is clearer when using the SG potential.

ACKNOWLEDGMENTS

This work was supported by the Russian Foundation for Basic Research, project no. 13-08-00273.

REFERENCES

1. E. Merian, *Metals and their Compounds in the Environment: Occurrence, Analysis, and Biological Relevance* (VCH Publ., Weinheim, 1991), p. 1438.
2. G. H. Fernandez-Leborans and O. Yolanda, Ecotoxicol. Environ. Safety **47**, 266 (2000).
3. A. Sayari, S. Hamoudi, and Y. Yang, Chem. Mater. **17**, 212 (2005).
4. R. Li, L. Liu, and F. Yang, Chem. Eng. J. **229**, 460 (2013).
5. J.-M. Bomont and J.-L. Bretonnet, J. Phys.: Conf. Ser. **98**, 042018 (2008).
6. J.-M. Bomont, J.-L. Bretonnet, D. J. Gonzalez, and L. E. Gonzalez, Phys. Rev. B **79**, 144202 (2009).
7. A. E. Galashev and V. A. Polukhin, Russ. J. Phys. Chem. A **88**, 995 (2014).
8. J. Tersoff, Phys. Rev. B: Condens. Matter. **37**, 6991 (1988).
9. J. Tersoff, Phys. Rev. B: Condens. Matter. **39**, 5566 (1988).
10. S. J. Stuart, A. V. Tutein, and J. A. J. Harrison, Chem. Phys. **112**, 6472 (2000).
11. F. Epstein and M. D. Powers, J. Phys. Chem. **57**, 336 (1953).
12. L. J. Munro and J. K. Johnson, J. Chem. Phys. **114**, 5545 (2001).
13. A. Kutana and K. P. Giapis, Nano Lett. **6**, 656 (2006).
14. P. Schwerdtfeger, R. Wesendrup, and G. E. Moyano, J. Chem. Phys. **115**, 7401 (2001).
15. F. D. Lamari and D. Levesque, Carbon **49**, 5196 (2011).
16. C. D. Wick, M. G. Martin, and J. I. Siepmann, J. Chem. Phys. B **104**, 8008 (2000).
17. S. Yu. Davydov, Phys. Solid State **54**, 875 (2012).
18. Y. S. Badyal, U. Bafile, K. Miyazaki, et al., Phys. Rev. E **68**, 061208 (2003).
19. V. V. M. Lobo and R. Mills, Electrochim. Acta **27**, 969 (1982).

Translated by A. Muravev